On the deformation behavior of bi - metal via digital image correlation

Yuliya Li[1,2*], Svetlana Barannikova[1,2], Lev Zuev[1,2]

[1] *National Research Tomsk State University, 36 Lenin Ave,Tomsk, 634050, Russia.*
[2] *Institute of Strength Physics and Materials Science, SB RAS, 2/4, pr. Akademicheskii, Tomsk, 634055, Russia*

DOI: 10.5185/amlett.2018.7069
www.vbripress.com/aml

Abstract

The aim of this contribution was to study the localization of the plastic deformation of bi - metal based on a low-carbon steel A 283 Grade C and austenitic stainless steel 301 AISI. The images of the localized zone plastic deformation upon the uniaxial tension have been obtained with using digital image correlation method (DIC). The stress-strain curves are found to show all the plastic flow stages: yield plateau, linear and parabolic work hardening stages and the prefracture stage would occur for the respective values of the exponent from the Ludwik-Holomon equation. The main parameters of plastic flow localization at various stages of the deformation hardening have been determined in bi - metal. Copyright © 2018 VBRI Press.

Keywords: Bi-metal, localization of the plastic deformation, DIC, plastic flow, auto waves.

Introduction

Scientists are continually searching to find new material with better properties for industrial application. **[1]** Ones new multi-layer materials are identified, machining and joining processes for them are also developed **[1-3]**. Bi - metal belong to these materials, which are composed of two metals and alloys.

The most important advantage is that cladding steel no only saves cost more than similar steels made entirely of cladding materials, but also provides other functions including good mechanical strength, good resistance to heat and corrosion. Therefore, it is widely used in petroleum, chemical, medicine, and nuclear industries **[4-7]**.

In this study, bimetal consisted of austenitic stainless steel 301 AISI and low-carbon steel A 283 Grade. Stainless steel has an excellent corrosion resistance and stability in gaseous and aqueous environment and an excellent specific strength compared to low carbon steel. Carbon steel has a good strength and an excellent cost advantage over stainless steel, but less environmental stability and corrosion resistance. Recently, the efforts to develop mechanically reliable stainless steel/carbon steel bimetal have increased considerably driven by the need for materials with excellent corrosion resistance, good environmental stability, high specific strength and low production cost **[8]**.

Multilayer metals exposed to extensive plastic deformation during operation. A limited number of investigations are devoted to deformation behaviors of bimetal. Currently, heterogeneity of plastic deformation at macro-, meso- and microscopic scale have been identified and studied for a wide range of pure metals and alloys **[9-12]**. At the macroscopic level the plastic deformation will exhibit an inhomogeneous localization behavior from yield stress to failure **[13]**. Various forms of this plastic deformation localization can be considered as different type of auto waves that depend on the strain hardening law taking place at the stage. According to early works **[14]**, focusing on the auto waves approach for the description of the localized plastic deformation of FCC, BCC and HCP of metals and alloys, are gathered with the use of the ALMEC-tv measuring complex for digital recording of speckle images, above-mentioned methods are proposed to study plastic flow localization in bimetals.

Experimental

Materials and fabrications

The investigations were performed for anticorrosive bi - metal are based on joining dissimilar metals: low-carbon steel A 283 Grade C and austenitic stainless steel 301 AISI. This two-layer composite was produced via pouring followed by rolling on a required thinness of 8mm. The thickness of the cladding layer was 0.6mm. Pouring liquid metal onto a solid plate placed in the mold is frequently used to fabricate various bimetals **[15]**.

Response measurements

Previously prepared in the form of dog bones, the specimens with dimensions of the working part 40 ×8×2 have been tensiled with testing machine LFM-125, at 300 K with a rate of 6.67×10^{-5} s^{-1}mm/min. The stress-strain curve was obtained simultaneously with measuring the fields of the displacement vectors r(x, y) with using of the universal measuring complex for digital recording of speckle images ALMEC-tv based on DIC method. This enabled to measure of displacement vector fields for the sample surface. The measurements were performed over

the entire plastic flow process from tensile yield point to fracture.

Use of this method makes it possible to determine the main characteristics of propagation of the zone of localized plastic deformation such as the spatial λ and temporal T period of the process.

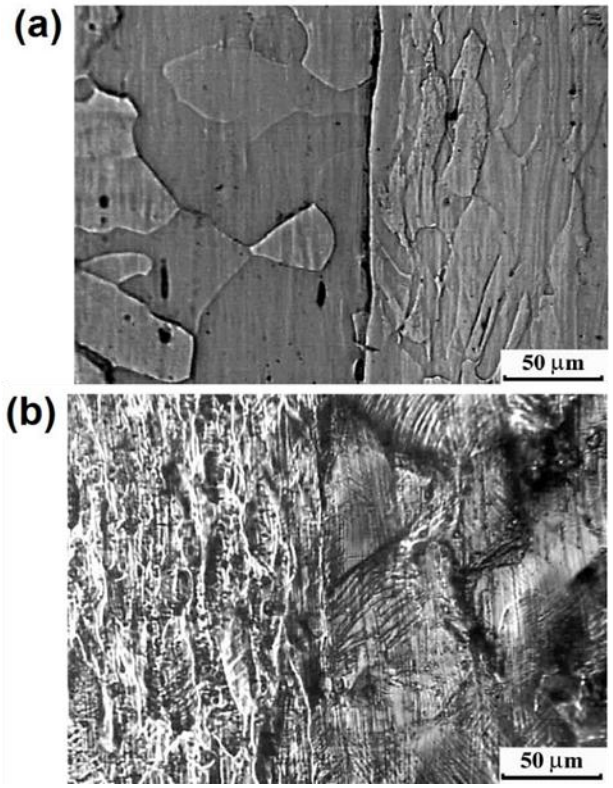

Fig. 1. Microstructure of bi-layered metal (a) before uniaxial tension; (b) after uniaxial tension.

Results and discussion

As a result of metallographic analysis, as shown in **Fig. 1(a)**, the initial state of metal structure (before uniaxial tension) was confirmed. It is characterized by a fusion line of the metal zone, free of defects, thus ensuring high mechanical properties. The bi –layered metal interface between the working part (cladding layer) from austenitic alloy steel and the bearing part (parent layer) from low carbon steel is evidently visible. The discontinuity flaw and foreign particulate were not detected along the full contact area of the bi -metal material. The grains of both the working part and bearing part are elongated along the rolling direction. The structure of the cladding layer stainless steel - 301 shows austenite grain elongated along the axis of rolling. A decarbonized layer was observed near the side of low- carbon steel, with the layer depths reaching about 250 μm. Microstructural examinations of the parent metal revealed that ferrite and perlite were the dominant structures in it.

Fig. 1(b) shows the deformational microrelief of the grain interface after the tensile test before the sample fractures. The intragranular shearing microrelief arises in both the working part and bearing part. This fact is related to single skidding and multiple skidding. The plastic deformation localization is accompanied by slip band formation on conjugate systems that occur in the decarbonized layer of parent metal A 283 Grade C. It displays the stress concentrators as a trihedral prism (**Fig. 1 (b)**).

The deformation curve upon the tension of the stainless steel 301 AISI – A 283 Grade C specimens are shown in **Fig. 2**. The plastic flow curve is attributed to the general diagrams described by the Lüdwig equation:

$$\sigma(\varepsilon) = \sigma_y + \theta\varepsilon^n$$

where, θ is the coefficient of deformation hardening and n is the exponent of deformation hardening. The strain exponent n has different values in different portions of the stress-strain curve and changes in a stepwise manner depending on the degree of strain. Particular constant values of n and θ correspond to each of the deformation stages.

An analysis of the loading curve shows that the specificity of this curve is the occurrence of yield plateau (2) and yield drop (1) **(Fig. 2)**. The extent of yield plateau with yield drop is 0.8%, that is conditioned by the propagation of the Lüders band in the base material (A 283 Grade C).

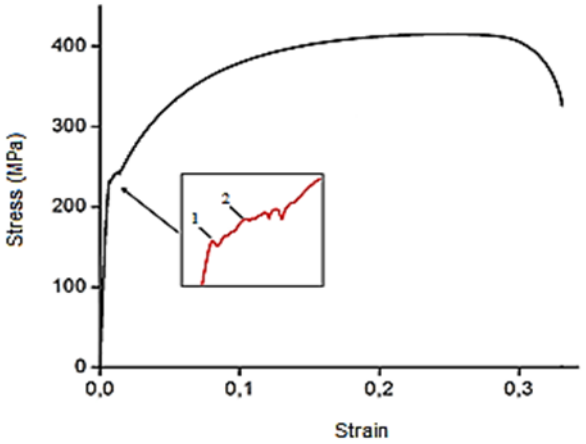

Fig. 2. Loading curves, the load curve under uniaxial tension: 1 yield drop; 2 - yield plateau.

The analysis of the stages in the loading diagrams of bimetal specimens from the work hardening coefficient $\theta = d\sigma / d\varepsilon$ and the constant value n (here is the exponent of deformation hardening in the Lüdwik equation) reveal the following peculiarities of the deformation curves for the material studied. The transition segment from the elastic part to the plastic flow is supervened by the yield plateau that changed by the linear-hardening stage with the total deformation of ε_{tot}= 3% ÷ 5.5%. The Taylor parabolic work-hardening stage with the constant n =1/2 and the total deformation of ε_{tot} =12% ÷ 20% comes after, and, finally, there is the prefracture stage with the constant n ~ 0.3 and total deformation of ε_{tot} = 24% ÷ 29%.

Copyright © 2018 VBRI Press

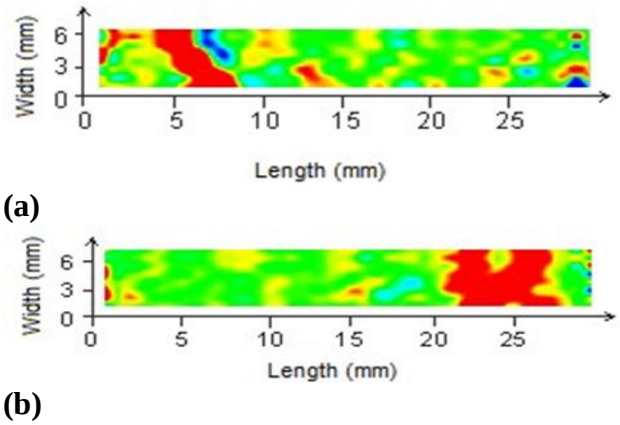

Fig. 3. Visualization of Lüders band propagation through the bimetal length at the total deformation of (a) 0.006 and (b) 0.012.

Plastic deformation of the composite emerges from the Lüders band interface in the bimetal. However, the stainless steel 301 AISI high-strength cladding metal prevents the propagation of the Lüders band with the constant velocity from the clamp of the machine as the basic stress concentrator. This results in the abrupt movement of the initial band with the origin and propagation of other Lüders bands through the specimen section from the cladding metal – basic metal interface **(Fig.3 (a)).** The emergence of the stress concentrators is caused by the bending moments that arise upon plastic deformation of the bimetal. The propagation of the local elongations on the yield plateau is the relay propagation of the Lüders band fronts emerging near the clamps and at the opposite interfaces. The Lüders fronts move and vanish when meeting each other on the yield plateau (**Fig. 3 (b)**).

The sequence of the plastic deformation localization zones is found at the linear deformation strengthening with the spatial period λ = 4 mm and their propagation velocity V_{aw}.= $6 \cdot 10^{-5}$ m/s **(Fig. 4)**.

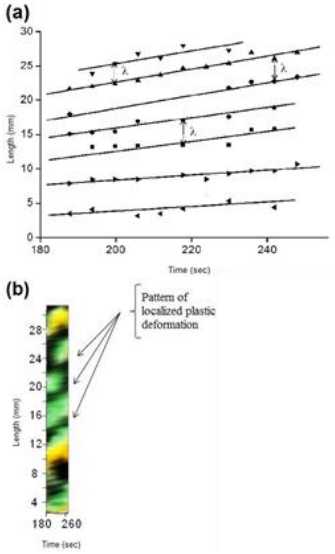

Fig. 4. Visualization of kinetic plot X(t) of strain localization zone along sample axis as functions of time – (a) and pattern of localized plastic deformation along sample – (b) at linear stage of deformation hardening.

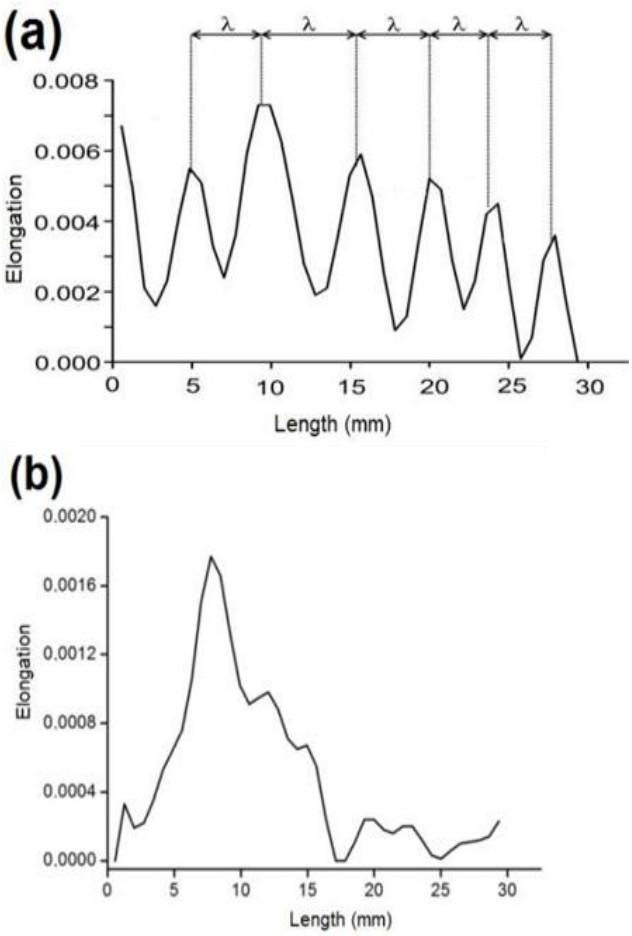

Fig. 5. The local elongation ε_{xx} along the axis of extension during (a) - parabolic strain hardening; (b) - prefracture stage.

The parabolic reveals plastic flow localization in the form of a stationary system of the plastic flow centers through the specimen length with the distance λ = 4 mm between them **(Fig. 5(a))**.

At the prefracture stage, the immobile zones of plastic strain localization started moving consistently with a tendency to merge into a high-amplitude focus of localized straining **(Fig. 5 (b))**, where a neck-like narrowing of the sample cross section was formed **(Fig. 6 (a, b))**. This maximum forms at the place of occurring damage. The peculiarity of damage of the bimetal is related to the heterogeneity of plastic deformation in the intermediate layer of the metal, where the stress concentrator as a trihedral prism is formed on microlevel **(Fig. 6 (a))**. Fragmentation of the specimen determines the fracture pattern of bimetal composite. Two macro bands of localized plastic deformation are formed at the stage of the shoulder effect in the area of stress macro concentrator. They propagate along conjugated directions of maximum shear stress across the whole section of the sample, forming trihedral prisms on the macro level on the bond interface of the bimetal. The cracks are nucleated in the area of parent metal at the trihedral prism tip, gradually merged passing across the whole section of the metal sample **(Fig. 6 (b)).**

Copyright © 2018 VBRI Press

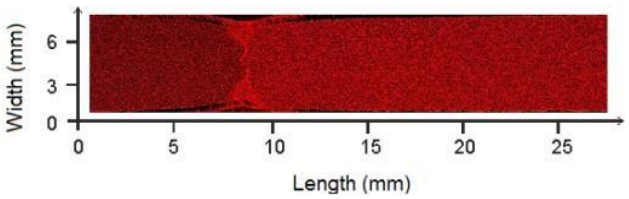

(a)

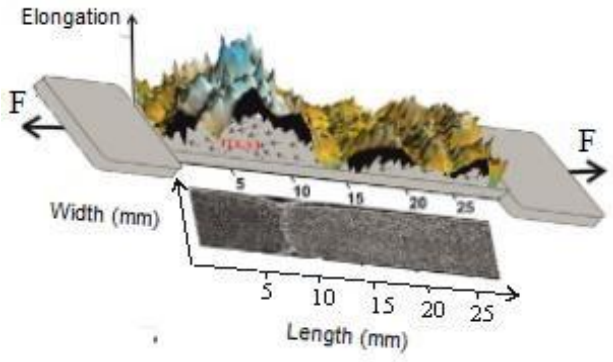

(b)

Fig. 6. The picture of localized zones evolution for parabolic work hardening and prefracture stages, under deformation 22% – (a); bimetal fracture patterns and distribution of local extensions at the prefracture stage under deformation 24%– (b).

The localized deformation patterns observed in most cases are ordered in space and with time; the pattern type is determined by the plastic flow law. It is shown that the dependency $V_{aw}\sim(\theta)^{-1}$ is valid for the linear work hardening stage alone, i.e. for $\sigma\sim\varepsilon$, which agrees with the data obtained for single Cu crystals by A. Acharya. The localized plasticity picture observed for the parabolic work hardening stage is composed of stationary zones and would remain unaltered. A similar observation is reported by other workers, e.g. A. Roth who also obtained a loading diagram of parabolic type.

Table 1. The propagation velocity V_{aw} and spatial period λ of the plastic deformation localization zones.

No.	Materials	λ, mm	$V_{aw} \cdot 10^5$, m/s
1.	Stainless steel [16]	4.0	3.5
2.	Low-carbon steel [17]	8.0	5.3
3.	Bi-metal	4.0	6.0

The propagation velocity V_{aw} and spatial period λ of the plastic deformation localization zones for the studied bi-metal as compared to stainless and low-carbon steels **[16, 17]** are given in **Table 1** to show satisfactory agreement with the universal inversely proportional relation between the macrolocalized plastic-strain autowave velocity and the work-hardening coefficient θ normalized by the shear modulus of the material **[10, 18]**. The shape of this dependence ($V_{aw} \sim 1/\theta$) is quite different from the well-known plasticity Kolsky waves described by the dependence $V_{pl} \sim \sqrt{\theta}$. The distinction between the above two dependences leads us to conclude that we have discovered a new type of wave processes upon the uniaxial tension with using digital image correlation method. They are self-excited waves of plastic flow. The localized plasticity picture observed for the parabolic work hardening stage is composed of stationary zones and would remain unaltered. A similar observation is reported in **[19]**.

The above complex deformation behavior of the bi - metal suggests that the appearance of the single localized maximum is a manifestation of significant changes in the material properties. This is indirectly indicated, for example, by the occurrence of an extremum, which appears, for example, on the plot of ultrasound rate against deformation a short time before necking is initiated in the tensile metals and alloys **[10]**.

The use of flow localization patterns allows one to reveal a jump-wise change of the plasticity of alloys shell at the initial stage of rolling, which is undetectable by any other means. In order to maintain uniform ductility over all material volume, an appropriate choice of dies and mandrel profiles is required or else a change in the reduction regime might be called for (see, e.g. **[20]**).

Conclusion

The characterization of the stainless steel – low-carbon steel composite upon uniaxial tension has enabled us to reveal the following features of the deformation of plastic bimetals. The zones of localized plastic deformation are formed and evolved during plastic flow in the basic metal. The cladding layer in the material prevents the propagation of the Lüders bands with a constant velocity from the machine clamp as the basic stress concentrator. The bands that have emerged move abruptly with the other Lüders bands from the cladding metal – basic metal inner interfaces and pass through the whole cross-section of the specimen. Fragmentation and destruction of the bimetal are caused by the formation of the stress concentrators at the cladding metal – basic metal inner interface.

The localization behavior of plastic deformation of bi-metal is its most salient feature. By constant-rate tensile loading, space-time periodic structures, which are called now patterns **[21]**, will emerge in the deforming sample from yield limit to failure of material. A total of four localized plasticity patterns have been observed experimentally for all studied materials which differ in chemical and phase composition, crystal lattice type (FCC, BCC or HCP), grain size and deformation mechanism **[10]**.

It is pertinent to remark that a detailed analysis of localized plasticity patterns serves to provide a unified explanation of the principal features of the deformation **[10],** which are as follows - localization structures will occur spontaneously in the sample by constant-rate loading in the absence of any specific action from without;

- in the course of plastic deformation, a changeover in the localized plasticity patterns is observed;
- for each flow stage there is only one kind of localization pattern;
- the emergence of such patterns is unrelated to deformation micro mechanisms or similar events;

Copyright © 2018 VBRI Press

- due to work hardening, the deforming medium's defect structure undergoes irreversible changes, which are reflected in the emergent patterns.

Acknowledgements

The work was performed in the frame of Fundamental Research Program of State Academy of Sciences for the period 2016-2020 yrs and it was supported by Tomsk State University competitiveness improvement programme (Project No. 8.1.14.2017).

References

1. Acarer, M.; Gulenc, B.; Findik, F; *Mater.Des.*,**2003**, 24, 659. **DOI:** 10.1016/S0261-3069(03)00066-9
2. Khadadad, A.; Kosak, M.; Ventzke, V; *Press. Vessel Pip*., **2002**, 79,181. **DOI:** 10.1016/S0308-0161(02)00012-1
3. Venkateswara, N.; Madhusudhan, G.; Nagarjuna, S; *Mater. Des*., **2011**, 32, 2496. **DOI:** 10.1016/j.matdes.2010.10.026
4. Findik, F.; Yilmaz, R.; Somyurek, T; *Acad. J*., **2011**, 19, 4141. **DOI:** 10.5897/SRE11.1018
5. Guobin, L.; Jianjun, W.; Xiangzhi, L.; Guiyun, L; *J. Mater. Proc. Technol*., **1998**, 75, 152. **DOI:** 10.1016/S0924-0136(97)00318-X
6. Mehnen, L.; Pfutzner, H.; Kaniusas, E; *J. Magn.Magn. Mater*., **2000**, 215, 779. **DOI:** 10.1016/S0304-8853(00)00286-9
7. Nakano, J.; Miwa, Y.; Tsukada, T.; Kikuchi, M.; Kita, S.; Nemoto, Y.; Tsuji, H.; Jitsukawa S; *J. Nucl. Mate*r., **2002**, 307, 1568. **DOI:** 10.1016/S0022-3115(02)00965-0
8. Akramifarid, H.R.; Mirzadeh, H.; Parsa, M.H; *Mater. Sci. Eng*., **2014**, A 613, 232. **DOI:** 10.1016/j.msea.2014.06.109
9. Barannikova, S. A; *Tech. Phys*., **2000**, 45, 1368. **DOI:** 10.1134/1.1318982
10. Zuev, L. B.; Barannikova, S. A; *Int. J. Mec. Sci*., **2014**, 88, 1. **DOI:** 10.1016/j.ijmecsci.2014.06.012
11. Mudrock, R.N.; Lebyodkin, M.A.; Kurath, P.; Beaudoin, A.; Lebedkina, T.A; *Scr. Mater*., **2011**, 65, 1093. **DOI:** 10.1016/j.scriptamat.2011.09.025
12. Tretiakova T.V.; Vildeman V.E; *Fratt. Integ. Strut*., **2013**, 24, 1. **DOI:** 10.3221/IGF-ESIS.24.01
13. Barannikova, S.A; Nadezhkin, M.V.; Zuev, L.B; *Techn. Phys. Lett*., **2011**, 37, 750. **DOI:** 10.1134/s1063785011080177
14. Barannikova, S.; Li, Y.; Malinovsky, A.; Pestsov D; *Key.Eng. Mat*., **2009**, 17, 1. **DOI:** 10.4028/www.scientific.net/KEM.683.84
15. Chen, L.; Yang, Z.; Jha, B.; Xia, G.;Stevenson, J.W; *J. Power Sources*, **2005**, 152**,** 40. **DOI:** 10.1016/j.jpowsour.2005.01.055
16. Zuev, L.B.; Barannikova, S.A.; Nadezhkin, M.V.; Mel'nichuk, V.A; *Techn. Phys. Lett.*, **2011**, 37, 793. **DOI:** 10.1134/S1063785011090057
17. Barannikova, S.A.; Kosinov, D.A.; Nadezhkin, M.V.; Lunev, A.G.; Gorbatenko, V.V.; Zuev, L.B.; Gromov, V.E; *Rus. Phys. J*., **2014**, 57, 396. **DOI:** 10.1007/s11182-014-0252-4
18. Acharya, A.; Beaudoin, A.; Miller, R; *Math. Mech. Sol*., **2008**, 13, 292. **DOI:** 10.1177/1081286507086903
19. Roth, A.; Lebedkina, T.A.; Lebyodkin, M.A*; Mater. Sci. Eng.* A. **2012**, 539, 280. **DOI:** 10.1016/j.msea.2012.01.094
20. Zuev, L.B.; Zykov, I.Yu.; Barannikova, S.A; *Adv. Mat. Res*., **2014**, 1040, 113. **DOI:**10.4028/www.scientific.net/AMR.1040.113
21. Aifantis, E.C. Gradient Plasticity in: J. Lemaitre (Ed.); Handbook of Materials Behavior Models; Academic Press: New York, **2001**, pp. 291-307.

Copyright © 2018 VBRI Press